Taylor Dispersion Analysis and Atomic Force Microscopy Provide a Quantitative Insight into the Aggregation Kinetics of Aβ (1–40)/Aβ (1–42) Amyloid Peptide Mixtures

Mihai Deleanu, Olivier Deschaume, Luca Cipelletti, Jean-François Hernandez, Carmen Bartic, Hervé Cottet, Joseph Chamieh

▶ To cite this version:

Mihai Deleanu, Olivier Deschaume, Luca Cipelletti, Jean-François Hernandez, Carmen Bartic, et al.. Taylor Dispersion Analysis and Atomic Force Microscopy Provide a Quantitative Insight into the Aggregation Kinetics of Aβ (1–40)/Aβ (1–42) Amyloid Peptide Mixtures. ACS Chemical Neuroscience, 2022, 13 (6), pp.786-795. 10.1021/acschemneuro.1c00784 . hal-03801189

HAL Id: hal-03801189

https://hal.science/hal-03801189v1

Submitted on 6 Oct 2022

Taylor Dispersion Analysis and Atomic Force Microscopy provide quantitative insight on the aggregation kinetics of Aβ(1-40)/Aβ(1-42) amyloid peptide mixtures

*Mihai Deleanu[1], Olivier Deschaume[2], Luca Cipelletti[3,4], Jean-François Hernandez[1], Carmen Bartic[2], Hervé Cottet[*1], Joseph Chamieh[*1]*

[1]IBMM, Univ Montpellier, CNRS, ENSCM, Montpellier, France

[2]Department of Physics and Astronomy, Soft-Matter Physics and Biophysics Section, KU Leuven, Celestijnenlaan 200D, Box 2416, 3001 Heverlee, Belgium

[3]L2C, Université Montpellier, 34095 Montpellier, France

[4]Institut Universitaire de France (IUF), France

[*] CORRESPONDING AUTHOR

Tel: +33 4 6714 3920, Fax: +33 4 6763 1046. E-mail: joseph.chamieh@umontpellier.fr

Tel: +33 4 6714 3427, Fax: +33 4 6763 1046. E-mail: herve.cottet@umontpellier.fr

ABSTRACT

Aggregation of amyloid β peptides is known to be one of the main processes responsible for Alzheimer's disease. The resulting dementia is believed to be due in part to the formation of potentially toxic oligomers. However, the study of such intermediates and the understanding of how they form is very challenging because they are heterogeneous and transient in nature. Unfortunately, few techniques can quantify, in real time, the proportion and the size of the different soluble species during the aggregation process. In a previous work (Deleanu *et al.* Anal. Chem. 2021), we showed the potential of Taylor dispersion analysis (TDA) in amyloid speciation during the aggregation process of Aβ(1-40) and Aβ(1-42). The current work aims at exploring in detail the aggregation of amyloid Aβ(1-40):Aβ(1-42) peptide mixtures with different proportions of each peptide (1:0, 3:1, 1:1, 1:3 and 0:1), using TDA and atomic force microscopy (AFM). TDA allowed for monitoring the kinetics of the amyloid assembly and quantifying the transient intermediates. Complementarily, AFM allowed the formation of insoluble fibrils to be visualized. Together, the two techniques enabled to study the influence of the peptide ratios on the kinetics and the formation of potentially toxic oligomeric species.

KEYWORDS. Taylor dispersion analysis; AFM; peptide aggregation; oligomers; amyloid beta peptides; diffusion coefficient; hydrodynamic radius.

Introduction

Alzheimer’s disease (AD) is the most common primary dementia. It usually presents a progressive course and characteristically affects different cognitive and behavioral functions. Perhaps the cardinal, most frequently observed symptom of disease onset is memory loss[1], which results from initial lesions in the hippocampus (which lies in the medial temporal lobes of the brain and is responsible for long-term memory) further extending to the rest of the brain. At later stages, the degeneration of other cognitive and behavioral areas is observed which will clearly indicate the type of dementia.

The brains of Alzheimer's patients present a series of characteristic hallmarks. First, neurofibrillary tangles composed of hyperphosphorylated tau protein are observed in neurons. Then, extracellular fibrillary structures called neuritic (or senile) plaques, that are due to the deposition of amyloid β peptides (Aβ), are observed[2]. In the 1990’s, it was believed that the senile plaques were the most pathogenic forms of the Aβ[3, 4], which resulted from the self-assembly of the two major amyloid peptides Aβ(1-40) and Aβ(1-42). During this self-assembly, species are formed with evolving morphology and size from oligomers, to protofibrils and finally to fibrils and plaques, through a highly complicated process.

More recent studies suggested that the main factor of AD pathogenesis was the formation of soluble oligomers of Aβ, which are believed to be more toxic than plaques because they are able to spread across neuronal tissue and bind to membrane receptors, including the prion protein, promoting neurotoxicity and synaptic loss[5-7]. However, in contrast to fibrils, which are highly stable and can be observed by microscopy, the soluble oligomers are more difficult to detect and to study in real time[8], since they are metastable, transient[8] and highly polydisperse in size. Studies have shown that Aβ(1-40) does not quantitatively form small oligomers during the aggregation process but rather goes from monomers to fibrils following a direct pathway[9, 10]. On the other hand, Aβ(1-42) goes through the formation of intermediate species with diverse sizes and shapes[11, 12]. Although these two amyloid peptides coexist *in vivo*[13, 14], most of the *in vitro* studies on Aβ were focused on the study of pure peptide solutions and only a small proportion of the vast AD literature was dedicated to mixtures of these peptides[15-18]. Many of the studies dealing with the mixtures were directed toward the kinetics of the aggregation process and more particularly the study of the amyloid fibers[15-17, 19-21] and very few toward the oligomeric structures[18]. The aggregation process in such mixtures was already studied by Thioflavin T fluorescence[17, 21], sedimentation[15], atomic force microscopy (AFM)[16, 19], nuclear magnetic resonance (NMR)[22, 23] or electron paramagnetic resonance[18] to name few methods. The results from these studies indicated that both Aβ(1-40) and Aβ(1-42) interact during the aggregation process, with cross seeding between peptides. However, some authors claimed that the fibrils are homomolecular[17] while others stated that heteromolecular[18] fibrils are obtained. In all cases, it was observed that the presence of Aβ(1-42) accelerated the aggregation of Aβ(1-40) and vice versa. To our knowledge, an in-depth study on the species present during the early stages of the aggregation of amyloid peptide mixtures does not exist to date. For that reason, and to help develop drug candidates targeting the toxic oligomers, new analytical methodologies are required to monitor and size the different species in real time.

In this context, Taylor dispersion analysis[24-26] (TDA) appears as a very promising alternative analytical method. In our previous report[27], we showed the ability of TDA to follow the aggregation process of amyloid peptides, using an extensive data treatment that revealed a complete picture of the aggregation process and allowed to size the transient structures. As described elsewhere, TDA allows to determine the molecular diffusion coefficient, D, and hydrodynamic radius, R_h, of a solute, including for mixtures, without any bias in size as compared to other sizing methods[28], since the small and the large solutes contribute proportionally to their mass abundance in the mixture[29]. The use of TDA in the field of protein aggregation presents several advantages[30-33]. It offers low sample consumption (less than 1 µL for the whole aggregation process), short analysis time allowing a high number of sampling points and real time monitoring of the aggregation, a wide range of sizing (from angstrom to sub-micron) allowing to size the monomers, oligomers and higher size soluble prefibrillar structures, together with a direct analysis without any sample pretreatment or filtration [34-36].

In this work, we used TDA to study peptide mixtures of Aβ(1-40) and Aβ(1-42) with the aim of revealing the size of the transient structures formed during the aggregation process. The results for selected time points were compared with those obtained by AFM to correlate the observations from these two independent techniques. AFM also allowed to study non-soluble fibrils, which cannot be sized or directly observed by TDA.

Materials and methods

Materials

Amyloid beta (1-40) (denoted Aβ(1-40) in this work) was prepared by fast conventional solid phase peptide synthesis (SPPS) using a *Fmoc* orthogonal strategy as described elsewhere[27]. Amyloid beta (1-42) (Aβ(1-42), batch number 100002591, >95%) was purchased from Bachem (Bubendorf, Switzerland). Sodium dihydrogen phosphate, tris(hydroxymethyl)aminomethane, hydrochloric acid fuming 37%, sodium chloride and sodium hydroxide were purchased from Sigma Aldrich (France). The ultrapure water used for all buffers was prepared with a MilliQ system from Millipore (France).

Peptide pretreatment

Both Aβ(1-40) and Aβ(1-42) were first pretreated independently as described elsewhere[37, 38]. Briefly, Aβ(1-40) and Aβ(1-42) were dissolved in a 0.10 % (m/v) and 0.16 % (m/v) NH_4OH aqueous solution respectively to reach a final peptide concentration of 2 mg/mL. The peptide solutions were then incubated at room temperature for 10 min, separated into several aliquots and freeze-dried. The aliquot volume was calculated in order to obtain 10 nmol of peptide in each Eppendorf tube. The lyophilized peptide aliquots were stored at -20 °C until further use.

Peptide aggregation study by Taylor dispersion analysis

Briefly, and as described thoroughly elsewhere[25, 29, 30, 39], Taylor dispersion analysis allows for the determination of the molecular diffusion coefficient of a solute which can be obtained from the band broadening resulting from the combination of the Poiseuille parabolic flow and the molecular diffusion by quantifying the temporal variance (σ^2) of the elution profile. For that, a Gaussian function is used to fit the experimental elution peak allowing to obtain the peak variance σ^2 and thus calculate the molecular diffusion coefficient, D, and consequently the hydrodynamic radius, R_h. When more than one size populations are present, a sum of Gaussian functions can be used to fit the experimental trace, or Constrained Regularized Linear Inversion (CRLI)[40] can be used to get the size distribution. For more details, the reader may refer to the supporting information for the theoretical aspects, equations and more details on the data processing.

TDA was performed on an Agilent 7100 (Waldbronn, Germany) capillary electrophoresis system using bare fused silica capillaries (Polymicro technologies, USA) having 40 cm × 50 µm i.d. dimensions and a detection window at 31.5 cm. New capillaries were conditioned with the following flushes: 1 M NaOH for 30 min; ultrapure water for 30 min. Between each analysis, capillaries were rinsed with 20 mM phosphate buffer, pH 7.4 (2 min). Samples were injected hydrodynamically on the inlet end of the capillary (44 mbar, 3 s, injected volume was about 7 nL corresponding to 1% of the capillary volume to the detection point). Experiments were performed using a mobilization pressure of 100 mbar. The temperature of the capillary cartridge was set at 37 °C. The vial carrousel was thermostated using an external circulating water bath 600F from Julabo (Germany). The solutes were monitored by UV absorbance at 191 nm. The mobile phase was a 20 mM, pH 7.4 phosphate buffer (viscosity at 37 °C is 0.7×10^{-4} Pa.s). To prepare the mixtures, freeze-dried mixed peptide aliquots were prepared so that the final sample would contain 13 nmol of total peptide except for the pure samples where the amount of peptide was of 10 nmol. First, each of the required stock aliquots (see previous section) were dissolved in 100 µL of 0.16% (m/v) NH_4OH to avoid aggregation during this step, and appropriate volumes were used to obtain the desired mixtures. The final aliquots were immediately subjected to freeze-drying and then stored at -20°C until further use. The resulting peptide powders were dissolved in 20 mM phosphate buffer at pH 7.4 to reach a final total peptide concentration of 133 µM : *i*) 100 % Aβ(1-40) contained 10 nmol of Aβ(1-40) dissolved in 75 µL of buffer; *ii*) 75 % Aβ(1-40) and 25 % Aβ(1-42) mixture contained 10 nmol of Aβ(1-40) and 3.33 nmol of Aβ(1-42) dissolved in 100 µL of buffer; *iii*) 50 % Aβ(1-40) and 50 % Aβ(1-42) mixture contained 6.67 nmol of each peptide and was dissolved in 100 µL of buffer; *iv*) 25 % Aβ(1-40) and 75 % Aβ(1-42) mixture contained 3.33 nmol of Aβ(1-40) and 10 nmol of Aβ(1-42) dissolved in 100 µL of buffer and finally *v*) 0 % Aβ(1-40) contained 10 nmol of Aβ(1-42) dissolved in 75 µL of buffer. After dissolution, the mixtures were immediately transferred to a capillary electrophoresis vial and incubated at 37°C in the capillary electrophoresis instrument carrousel. Aggregation was monitored by injecting the sample ($V_{inj} \approx 7$ nL) every 7 min in the case of pure Aβ(1-42) and the Aβ(1-40): Aβ(1-42) 1:3 mixture (25 % Aβ(1-40)), while it was injected every 20 min for the Aβ(1-40): Aβ(1-42) 1:1 mixture (50 % Aβ(1-40)) and every 30 min in the case of pure Aβ(1-40) and the Aβ(1-40): Aβ(1-42) 3:1 mixture

(75 % Aβ(1-40)). During the monitoring of the aggregation process, each sample was injected for 100 to 125 TDA runs, corresponding to a total injected sample volume between 700 nL and 875 nL. To avoid sample evaporation, the vial cap was changed three times a day. The taylorgrams were recorded with the Agilent Chemstation software, then exported to Microsoft Excel for subsequent data processing. In general, the obtained elution profiles were not Gaussian, meaning that the sample was polydisperse in size. All taylorgrams were fitted on the basis of the right-side elution profile (*i.e.* $t > t_0$, with t_0 the peak time) to remove the spikes present on the left side as described elsewhere[27].

Atomic force microscopy (AFM)

For atomic force microscopy characterisation, 5 μL aliquots of the peptide solutions collected at different aggregation times were dried on silicon substrates freshly cleaned with piranha solution, before gently rinsing with ultrapure water and drying in a flow of nitrogen gas. An Agilent 5500 AFM system with MSNL-F cantilevers (f = 110-120 kHz, k = 0.6 N/m, average tip radius of 2-12 nm) was used for topographical imaging in intermittent contact mode. The AFM topography images were levelled, line-corrected and analysed using Gwyddion[41], a free and open-source SPM (scanning probe microscopy) data visualization and analysis program. Maxima analysis was performed using ImageJ[42].

Results and discussion

Taylor Dispersion Analysis and data processing

One main objective of this work is to show the influence of the relative proportion of Aβ(1-40) with respect to Aβ(1-42) on the aggregation process. The aggregation of the peptides in the different mixtures was followed at 37°C. Figure 1 shows the taylorgrams recorded at selected incubation times for Aβ(1-40), Aβ(1-40):Aβ(1-42) mixtures (with molar ratio of Aβ(1-40) in the mixture of 25%, 50% and 75% corresponding to 3:1, 1:1 and 1:3 mixtures), and Aβ(1-42). The total peptide concentration in each solution was set at 133.3 μM. All experimental taylorgrams, for all incubations times t_{ag}, are shown in Figures SI.1 to SI.5. Figure 1 allows for a visual comparison of the aggregation kinetics between the different amyloid peptide ratios. The absorbance decrease of the elution profile with t_{ag}, which is due to the decrease in concentration of the soluble species, was faster when increasing the Aβ(1-42) content in the mixture, as previously observed for pure peptide solutions[27].

In order to elucidate the aggregation process in these solutions, an extensive data treatment was realized on all the obtained taylorgrams. As already observed in our previous report[27], sharp peaks or spikes, sometimes appear on the left side of the elution peak because of the presence of large fibrils in suspension which are out of the Taylor regime[43, 44] and/or due to specific hydrodynamic behavior for suspended large aggregates[45]. The presence of these spikes imposes a data treatment on the right side of the elution profile. Two different approaches were used to treat the experimental elution profiles. First, the fitting with a finite number of Gaussian functions ($n = 4$ in this work), leads to the classification of the obtained size populations into four categories: (*i*) small unidentified molecules ($R_h < 0.9$ nm), (*ii*) monomers and small oligomers (0.9 nm $< R_h <$ 5 nm), (*iii*) higher mass oligomers (5 nm $< R_h <$ 50 nm) and finally (*iv*) soluble protofibrils (50 nm $< R_h$ $<$ 300 nm). The second approach is based on the Constrained Regularized Linear Inversion (CRLI) which aims at finding the probability density function $P_D(D)$ that fits the taylorgram without any hypothesis on the number of populations[40].

Aggregation process of pure and mixed solutions of Aβ peptides by TDA and AFM

In the case of Aβ(1-40) alone, the first sign of spikes (fibrils) appears at $t_{ag} \sim 12$ h (Figure SI.1). However, the spike intensity remained relatively low and did not increase drastically over the whole aggregation process (see gray data points in Figure 2). In parallel, the monomer peak intensity remained constant until $t_{ag} \sim 20$ h ("lag phase"), and then decreased rapidly to reach a lower plateau after $t_{ag} \sim 48$ h (red squares in Figure 2). This suggests an initial slow aggregation step followed by a rapid fibrillization catalyzed by the formation of large aggregates (seeds) that do not enter the capillary upon injection[46], in accordance with our previous report where another concentration (100 μM) of Aβ(1-40) was used[27].

On the contrary, Aβ(1-42) alone did not show any lag phase and a fast decrease of this population was observed with a complete disappearance after less than 2 h (red squares in Figure 2). Meanwhile, when mixed together, Aβ(1-42) seemed to increase the kinetics of aggregation, with the monomer population decreasing after 15 h, 8 h and 6 h for the 75%, 50% and 25% Aβ(1-40) mixtures respectively, without any visible lag phase (red squares in Figure 2).

With the aim of verifying hypotheses formulated from TDA, we also performed AFM imaging for key times of the fibrillization process. The findings by TDA correlated well with AFM observations for Aβ(1-40) alone (Figure 3), which showed the number of fibrils rise only at t_{ag} = 28.10 h. In AFM images, the substrate remained covered with spherical objects in the 10 nm diameter range (including eventual tip convolution effects) that can be attributed to monomers and oligomers. The coverage by these species only decreased significantly, exposing portions of the bare substrate, for t_{ag} = 28.10 h, which demonstrates the consumption of these objects by the fibrillization process.

In the case of Aβ(1-42) alone, the kinetics of aggregation were much faster than that of Aβ(1-40), as demonstrated by the taylorgrams (Figure 1) and the monomer consumption (red squares in Figure 2). The first spikes were observed only after t_{ag} ~ 10 min (Figure SI 5), in agreement with AFM showing fibrils for the shortest incubation times, and a complete disappearance of the soluble peptide species was observed after t_{ag} ~7 h (Figure 3). Similarly, only few monomeric/oligomeric species remained visible after 48 min in AFM images, which showed from this time onward mainly the substrate and fibrils. The decrease in the number of fibrils observed by microscopy for the longest incubation times is likely due to the tangling of fibrils and compaction of these aggregates, that have less affinity for the substrate and are more easily removed during the rinsing and drying steps, as observed for other amyloid systems[47].

When mixed together, aggregation/fibrillization observed by both TDA and AFM accelerated with the proportion of Aβ(1-42). In the case of the 75% Aβ(1-40) mixture, the first spikes in TDA appeared after t_{ag}~6.5 h (Figure SI.2), while they were observed after only ~1.5 h and ~1 h for the 50 % and 25 % Aβ(1-40) mixtures respectively (Figures SI.3 and SI.4 respectively). In the case of the mixture with the highest amount of Aβ(1-40), the spikes intensity increased with time and remained visible even after 60 h of aggregation suggesting that the formed fibrillary structures are smaller in size than those formed with Aβ(1-40) alone, and can enter more easily in the capillary during the injection step. These observations were also conveyed in the AFM images, with fibers appearing increasingly early during the aggregation process, and the spherical objects attributed to monomers and oligomers being consumed faster upon raising the proportion of Aβ(1-42). Indeed, these small species remain predominant on the substrates up to 28.10, 8.15, 3.05 and 0.27 h respectively for 0, 25, 75 and 100% Aβ(1-42).

As mentioned earlier, the Taylorgrams were treated by fitting a sum of Gaussian functions to extract the abundance of size populations present under each elution peak during the aggregation process. Figure 4 shows the hydrodynamic radii of the populations in the studied mixtures as a function of incubation time, while Table 1 shows the average hydrodynamic radii values for the size populations and the different peptide mixtures. As can be seen in Figure 4, the size of each population was relatively constant during the aggregation process. The population called 'monomer' corresponds to the monomers and small oligomers with an average size of about 2 nm in all mixtures. However, the statistical analysis showed that the monomer populations in Aβ(1-40) and in the 25 % Aβ(1-40) mixture were significantly smaller at a 95% confidence level than for the other three mixtures, based on the average hydrodynamic radii obtained over the whole aggregation study for each mixture (see Table 2 and Figure SI.6). Further, Aβ(1-40) alone showed the lowest 'monomer' population size average value of 1.81 ± 0.11 nm, while the 25 % Aβ(1-40) mixture showed the highest average value of 2.42 ± 0.20 nm. While the other three mixtures, 75 % Aβ(1-40) mixture, 50% Aβ(1-40) mixture and Aβ(1-42) alone were not statistically different (see R_h values in Table 2). These results suggest that when the mixture contained an excess of Aβ(1-42) as compared to Aβ(1-40), the formed oligomers were larger in size than those obtained for Aβ(1-42) alone and for the mixtures with a higher amount of Aβ(1-40). To explain this observation, the following hypothesis is proposed. First, it was already shown that Aβ(1-40) mainly forms fibrils directly from the monomeric state without passing through intermediate species[9, 10]. The presence of the first fibrils of Aβ(1-40) catalyzed by the presence of Aβ(1-42) may play the role of seeds for the Aβ(1-42) peptide[21], and thus, oligomers with a higher molar mass are formed. When the amount of Aβ(1-42) decreases, the aggregation process tends to follow the pathway characteristic of Aβ(1-40) (direct formation of fibrils), and thus, the smallest oligomeric species tend to remain monomeric with a lower average size. For AFM, in the presence of biomolecules, the lateral dimensions are often affected by tip convolution, leading to unpredictable broadening of surface features[48, 49]. We therefore measured the average heights of the various objects, which gave a good estimation of radii. The results obtained on the different mixtures of the radii (at times enabling to measure isolated objects) for small spherical objects attributed to monomers/oligomers, and the derived half-widths for the fibers are gathered in Table 2. The radii of monomers/oligomers are in good agreement between TDA and AFM, although values measured for monomers, oligomers and fibers with AFM are not significantly different between ratios.

Table 2: Average hydrodynamic radius in nm obtained by TDA over the whole aggregation process of each mixture. Average heights in nm obtained by AFM on the small spherical objects and on the fibrils for the different Aβ mixtures and at different aggregation times.

	TDA	**AFM**			
		Small spherical objects		**Fibrils**	
% Aβ(1-40) in Aβ(1-40):Aβ(1-42) mixtures	**Average R_h (nm) (*n*= number of points)**	**Radii ± SD (nm)**	**t_{ag} (h)**	**Half-width ± SD (nm)**	**t_{ag} (h)**
0	1.96 ± 0.10 (*n* = 121)	2.15 ± 0.40	1.47	2.89 ± 0.70	0.8
25	2.42 ± 0.20 (*n* = 77)	2.22 ± 0.44	8.02	2.78 ± 0.72	27.83
50	2.00 ± 0.25 (*n* = 42)	N.A.	N.A.	N.A.	N.A.
75	1.98 ± 0.24 (*n* = 77)	2.32 ± 0.44	12.23	3.02 ± 1.17	27.97
100	1.81 ± 0.11 (*n* = 53)	2.43 ± 0.60	28.10	3.53 ± 0.93	28.10

As for the higher mass oligomer population, the size remained relatively constant throughout the aggregation process within a given mixture. However, it was observed that with an increase in the Aβ(1-40) proportion, the average size for the oligomer population was higher than in the case of an excess of Aβ(1-42) (~18 nm as compared to ~9 nm) (Figure SI.6). Moreover, a sudden increase of the oligomer R_h from about 10 nm to ~ 30 nm can be observed when the "monomer" population decreased in area (Figure 2 for the size and Figure 4 for the area) after ~ 2h for Aβ(1-42), 24 h for the 75% Aβ(1-40) mixture and 32 h for Aβ(1-40). This effect was not observed for the 50% and 25% Aβ(1-40) mixtures. Further, Figure 2 shows that this oligomeric population reaches a maximum in concentration at around 30 min for the Aβ(1-42) sample, while this maximum is shifted to higher times with the decrease in Aβ(1-42) proportion (1.3 h, 1.6 h, 5.5 h and 16 h for 25%, 50%, 75% and 100 % Aβ(1-40) mixtures, respectively). Recent studies suggested that amyloid peptides can undergo liquid-liquid phase separation (LLPS) before the formation of amyloid fibrils[50-52]. The "high mass oligomers" population with R_h ranging from 5 to 50 nm found in this work, might correspond to high-density protein condensates. The size increase of the species over time can be explained by Ostwald ripening.

Regarding the protofibril population, the R_h values varied between 80 and 140 nm, for all the mixtures independently of the peptide proportions (Figure 4).

Hydrodynamic radius distributions by CRLI

To get a deeper insight into the evolution of the species during the aggregation process, CRLI analysis[27, 40] was applied on the right part of the taylorgrams (i.e. for $t > t_0$). Figure 5 shows the hydrodynamic radii distributions obtained by CRLI on TDA runs for selected aggregation times for all studied samples, while Figures SI.7 to SI.11 show the distributions over the whole aggregation process for the studied samples. From these distributions, one can note that for Aβ(1-40) alone, only the monomer and small oligomer populations were observed throughout the aggregation process without the notable appearance of intermediate species. On the contrary, Aβ(1-42) aggregation led to intermediate oligomers having an average size around 10 nm accompanied with a broadening and disappearance of the monomeric population in accordance with our previous report[27]. When mixed together, the presence of intermediate species became more noticeable with the increase in Aβ(1-42) proportion. These results provide an explanation to the increase in Aβ mixtures toxicity with an increase in the Aβ(1-42)/Aβ(1-40) ratio[19, 23, 53], supporting the notion that this toxicity correlates with the amount of intermediate oligomeric species.

Kinetic analysis of the aggregation process

One of the major advantages of using TDA combined with advanced data treatment is the possibility to get the size distributions of the different populations with high throughput during the whole aggregation process. These distributions allow gaining insight on the aggregation mechanism, by modelling the data based on the chain of association and dissociation reactions shown in Figure 6[54].

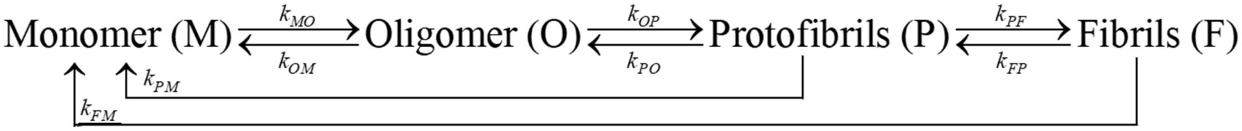

Figure 6. Scheme of the association and dissociation reactions of amyloid species used to model the aggregation process (adapted from[54]). The rate constant for each reaction is indicated close to the respective reaction arrow.

The forward and backward reactions going from the monomer (M) population to the oligomers (O), the protofibrils (P), and finally the fibrils (F), as shown in Figure 6, are modelled by the following set of equations:

$$\frac{dM(t)}{dt} = -k_{MO}M(t) + k_{OM}O(t) + k_{PM}P(t) + k_{FM}F(t) \qquad (1)$$

$$\frac{dO(t)}{dt} = -\left(k_{OP} + k_{OM}\right)O(t) + k_{MO}M(t) \qquad (2)$$

$$\frac{dP(t)}{dt} = -\left(k_{PF} + k_{OM}\right)P(t) + k_{OP}O(t) \qquad (3)$$

$$\frac{dF(t)}{dt} = k_{PF}P(t) - k_{FM}F(t) \qquad (4)$$

where, M(t), O(t), P(t) and F(t) are the concentrations of the monomers, oligomers, protofibrils and fibrils respectively. k_{MO} is the rate for the reaction transforming monomers into oligomers; similar notations are used for the other rate constants. Note that TDA does not allow the fibrils population to be directly measured, so only equations (1-3) were used. We fit Eqs. (1-3) to the temporal evolution of the population distributions obtained by TDA, by assuming that the (integrated) absorbance signal for each species is proportional to its concentration, and that the same proportionality constant applies to all species. Equation (4) was not used since TDA does not allow the direct quantification of the fibril concentrations. The fit is performed using custom software based on the Scipy package[55], performing a least square minimization of the set of rate constants, solving numerically Eqs. (1-3) at each iteration. The resulting fitting curves are shown as dot-dashed lines in Figure 2 (see also Figures SI.12 to SI.16), while the fitting parameters are reported in Table 1. Note that for most samples the monomer population asymptotically tends for large *t* to a non-zero concentration value, due to the dissociation of the higher-order species. The 100 % Aβ(1-40) could not be fitted entirely, because of the presence of a lag phase at early times.

However, data for this sample could be fitted by excluding the monomer population data points for $t < \sim 20$ h. For all other sample mixtures, the fit allowed to extract the kinetics rate constants reported in Table 1. From these values, it can be deduced that the reaction rates tend to decrease with increasing amounts of Aβ(1-40) in the mixture. For the 0% Aβ(1-40) sample, the forward reactions were dominant as compared to the backward ones, suggesting that the aggregation is close to an irreversible reaction rather than to an equilibrium one. When a small amount of Aβ(1-40) is added (25%), the reaction rates of forward and backward reactions become similar. These results can explain the higher toxicity of this Aβ ratio observed in the literature[19]. Indeed, the backward reactions correspond to the dissociation of higher order species into monomers or low molar mass oligomers, which are known to be toxic. To our knowledge, this is the first time that kinetic rates of the aggregation mechanism of Aβ peptides could be determined by measuring directly the monomer and oligomer distributions. When combined with models proposed in the literature, mainly based on measurements of the time-dependent aggregate mass [54, 56, 57] (e.g. by ThT fluorescence assay), or numerical simulations[58], TDA data as those presented here will help reaching a comprehensive understanding of the aggregation process of these amyloid species, potentially contributing to assess the effectiveness of drugs targeting the toxic oligomeric species.

Conclusion

This work demonstrated the interest of Taylor dispersion analysis to assist the study of complex amyloid peptide mixtures and shed more light on the aggregation process in these systems. The comparison of the results obtained in parallel by TDA and AFM showed the complementarity of the two techniques, where TDA is able to quantify and size of small objects while AFM can size the fibrillary structures not accessible by TDA. In addition, the results confirmed that the kinetics of aggregation strongly depend on the nature of amyloid-forming peptides and their environment. Under our working conditions, the more amyloid-prone Aβ(1-42) aggregates more rapidly (minutes scale) compared to Aβ(1-40), which aggregates in about 24h, in agreement with previously published works[27, 59]. When mixing together the two species, the aggregation rate was highly influenced by the ratio of Aβ(1-40):Aβ(1-42). Indeed, Aβ(1-42) was found to accelerate the aggregation rate of Aβ(1-40), probably by a cross-seeding mechanism. For example, the disappearance of the monomeric species decreased from 48 h in the case of 100 % Aβ(1-40) to 12 h when 25 % of Aβ(1-42) were present in the sample.

In addition to the clear observation on the interplay between both Aβ peptides during the aggregation process of mixtures and the influence of the Aβ ratio on the aggregation rate, this work shows that this ratio modulates the formation of potentially toxic oligomers. In fact, when the peptides were mixed together, intermediate oligomeric species were observed and tended to increase in proportion upon increasing the Aβ(1-42) content. Modifying the Aβ ratio changed the onset of the oligomeric species appearance and monomeric species disappearance (monomers and small oligomers R_h lower than 5 nm), as well as the aggregation mechanism (direct formation of fibrils or formation of intermediate species). These results support the importance of understanding the mechanism of the aggregation process in the case of Aβ mixtures (in better accordance with the *in vivo* conditions), to better direct research toward an AD therapy able to inhibit the formation of intermediate species depending on the Aβ ratio. In this respect, TDA was shown to be a straightforward method able to give with unprecedented detail new insight on the size and distribution of the species formed during the aggregation process. Finally, the combination of TDA with extensive data processing and highly resolved efficient methods such as AFM paves the way for building a comprehensive picture of the speciation and growth processes, as illustrated here for amyloid peptides, with potential applications to a wide range of biological, organic and inorganic polymer systems.

Table 1. Dependence of various parameters on the proportion of Aβ(1-40) in the studied mixtures. Populations' size: Average hydrodynamic radii of the monomer, oligomers and protofibrils size populations obtained by the deconvolution of the taylorgrams with a finite number of Gaussian functions. Kinetics parameters: values of the rate constants *k* obtained by fitting the peak areas corresponding to the various populations with equations (1) to (3). The last two columns show the time at which the oligomer population reaches its maximum, $t_{oligomers,max}$, and the initial concentration of the monomer population, M(t=0).

	Populations' size						***Kinetic parameters***							
% Aβ(1-40) in Aβ(1-40):Aβ(1-42) mixtures	***Monomer and small oligomers***		**Higher mass oligomers**		**Protofibrils**		***Forward reactions***			***Backward reactions***				
	<R_h> (nm)	**± SD**	**<R_h> (nm)**	**± SD**	**<R_h> (nm)**	**± SD**	**k_{MO} (h^{-1})**	**k_{OP} (h^{-1})**	**k_{PF} (h^{-1})**	**k_{OM} (h^{-1})**	**k_{PM} (h^{-1})**	**k_{FM} (h^{-1})**	**$t_{Oligomers,}$ max (h)**	**M(t=0) (mAU.min)**
100%	2.0	0.1	13.0	8.5	101.2	57.8	*N.A.*	*N.A.*	*N.A.*	*N.A.*	*N.A.*	*N.A.*	*N.A.*	*N.A.*
75%	2.4	0.2	9.3	1.8	140.2	43.7	1.106	0.817	0.943	1.497	0.123	0.050	4.171	3.551
50%	2.0	0.2	13.1	10.2	89.5	39.4	0.182	0.240	0.171	0.179	0	0.018	0.884	4.268
25%	2.0	0.2	17.9	10.4	135.6	56.9	1.457	1.226	2.190	1.386	1.332	0.045	0.722	3.709
0%	1.8	0.1	19.1	9.8	99.5	40.7	2.991	3.409	3.704	0	0.998	0.048	0.309	4.346

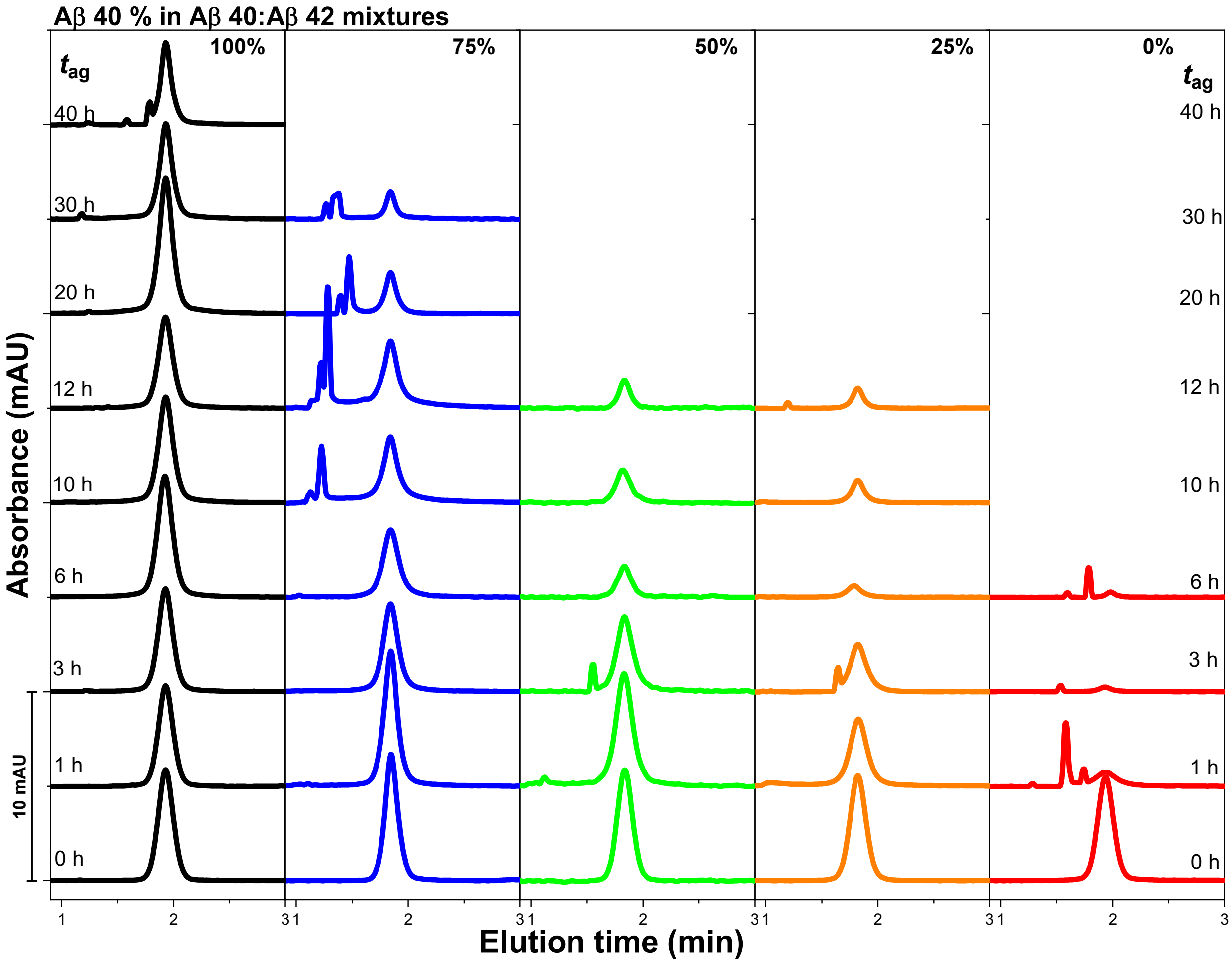

Figure 1. Overview of selected taylorgrams obtained during the aggregation process of Aβ(1-40) :Aβ(1-42) mixtures (Aβ(1-40) % of 100 %; 75%; 50%; 25% and 0%) at different common incubation times. Experimental conditions: Sample: 133 µM of total peptide; 20 mM phosphate buffer, pH 7.4. Incubation: quiescent conditions at 37 °C. Fused silica capillaries: 50 µm i.d. × 40 cm × 31.5 cm. Mobile phase: 20 mM phosphate buffer, pH 7.4. Mobilization pressure: 100 mbar. Injection: 44 mbar for 3 s, $V_i \approx 7$ nL (V_i / V_d $\approx$ 1 %). Analyses were performed at 37 °C. UV detection at 191 nm.

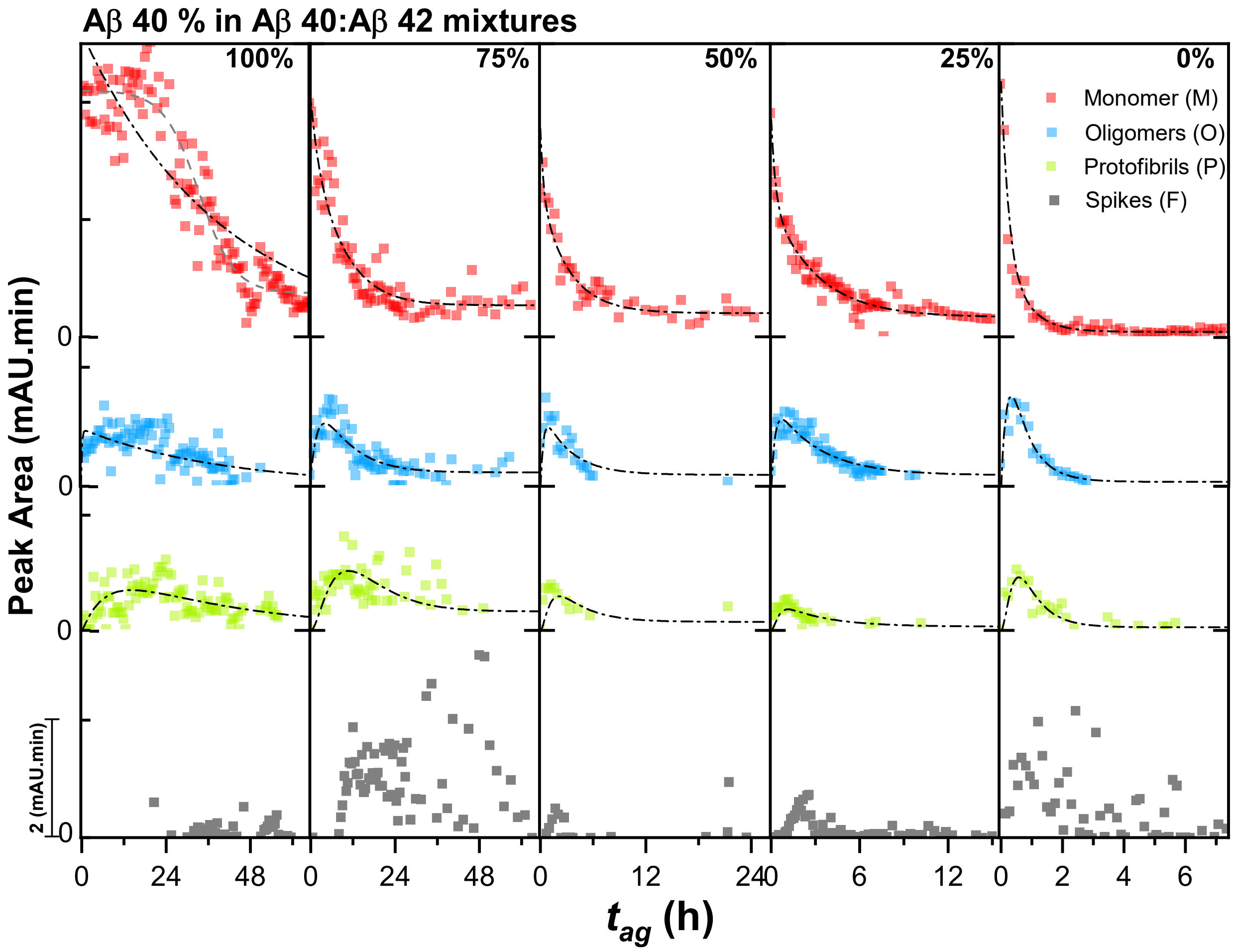

Figure 2. Peak area evolution of the different populations observed during the aggregation process of Aβ(1-40):Aβ(1-42) mixtures and obtained using a fit with finite number of Gaussian functions. Three size populations are represented: monomer and low molar mass oligomers (🟥), higher molar mass oligomers (🟦), soluble protofibrils (🟩) and non-diffusing species ("spikes") (■). Experimental conditions as in Figure 1. Black dashed-dotted lines are the kinetic fits obtained from equations (1) to (3). The grey dashed line in Aβ(1-40) monomer distribution is a guide for the eye. The scale of the vertical axis is the same in all graphs and is indicated on the bottom-left corner of the figure.

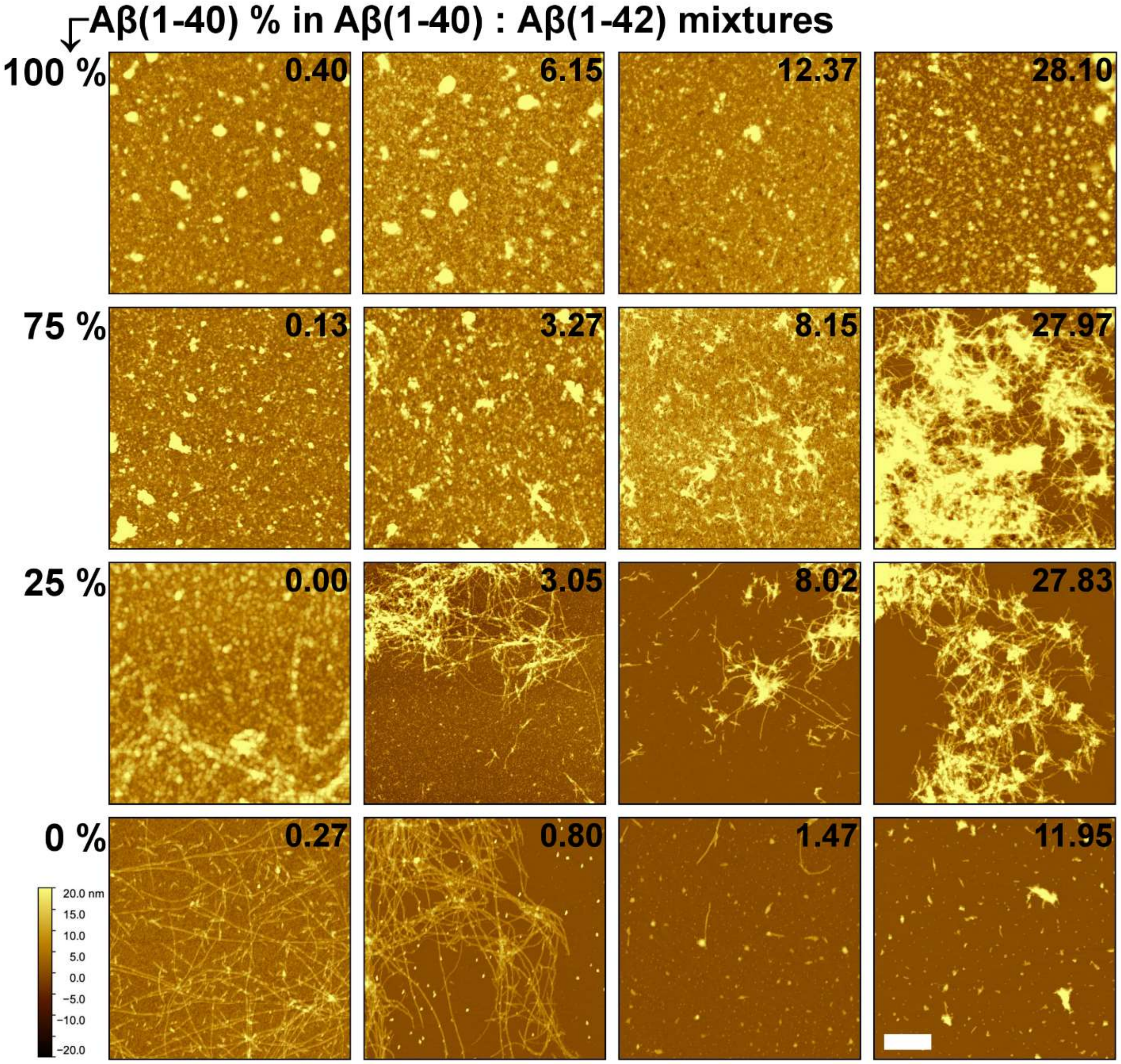

Figure 3: AFM images taken in intermittent contact mode under dry conditions, for different key times of the aggregation process in the presence of different peptide proportions. The Aβ(1-40):Aβ(1-42) ratio is given on the left side of the panel, aggregation times in hours are overlayed on the images. The scale bar on the bottom right corner is valid for all images and equals 1 µm.

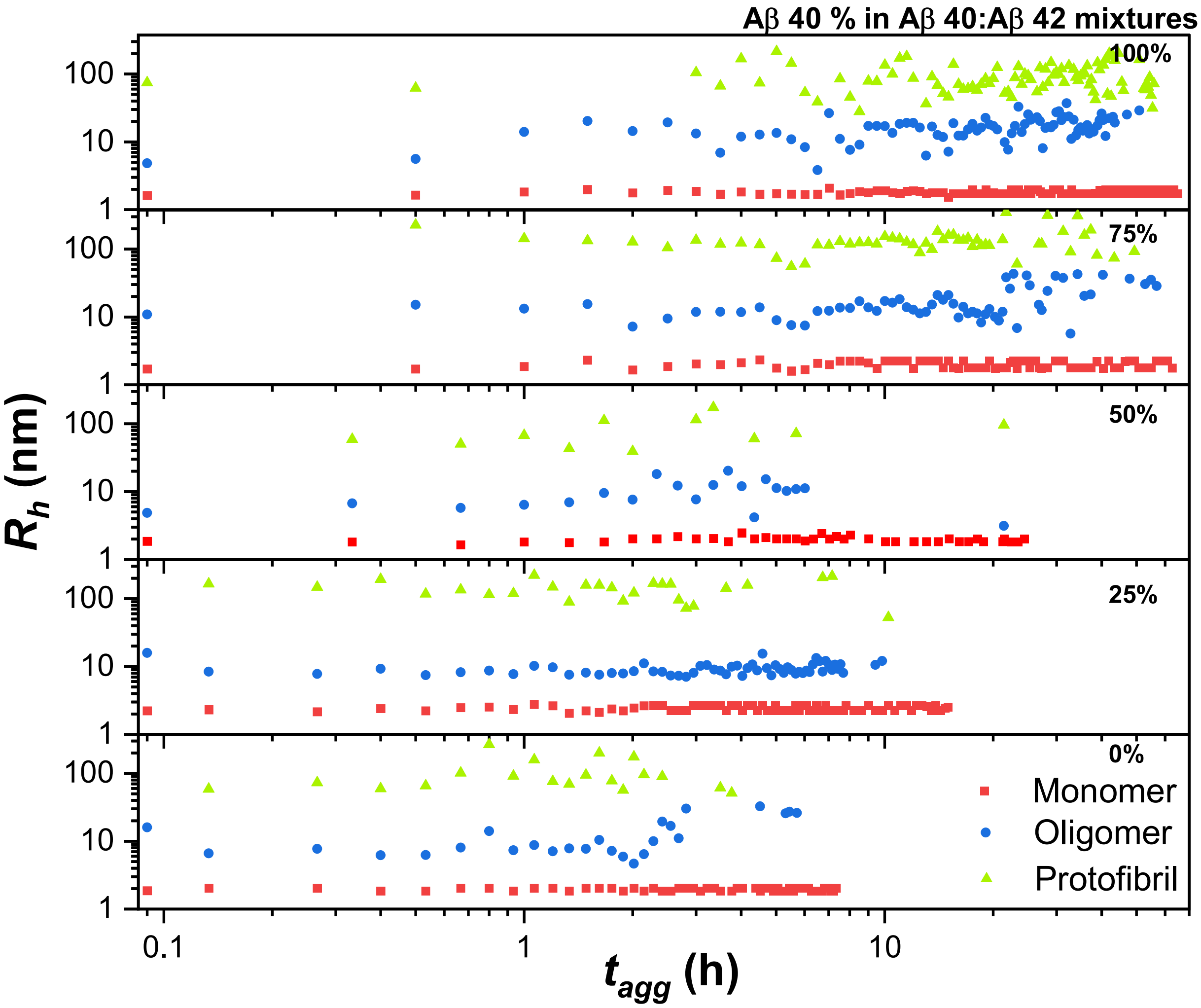

Figure 4. Hydrodynamic radius evolution of the different populations observed during the aggregation process of Aβ(1-40):Aβ(1-42) mixtures and obtained using a fit with finite number of Gaussian functions. Three size populations are represented: monomer and low molar mass oligomers $0.9 < R_h < 5$ nm (■), higher molar mass oligomers $5 < R_h < 50$ nm (●), and soluble protofibrils $50 < R_h < 300$ nm (▲). Experimental conditions as in Figure 1.

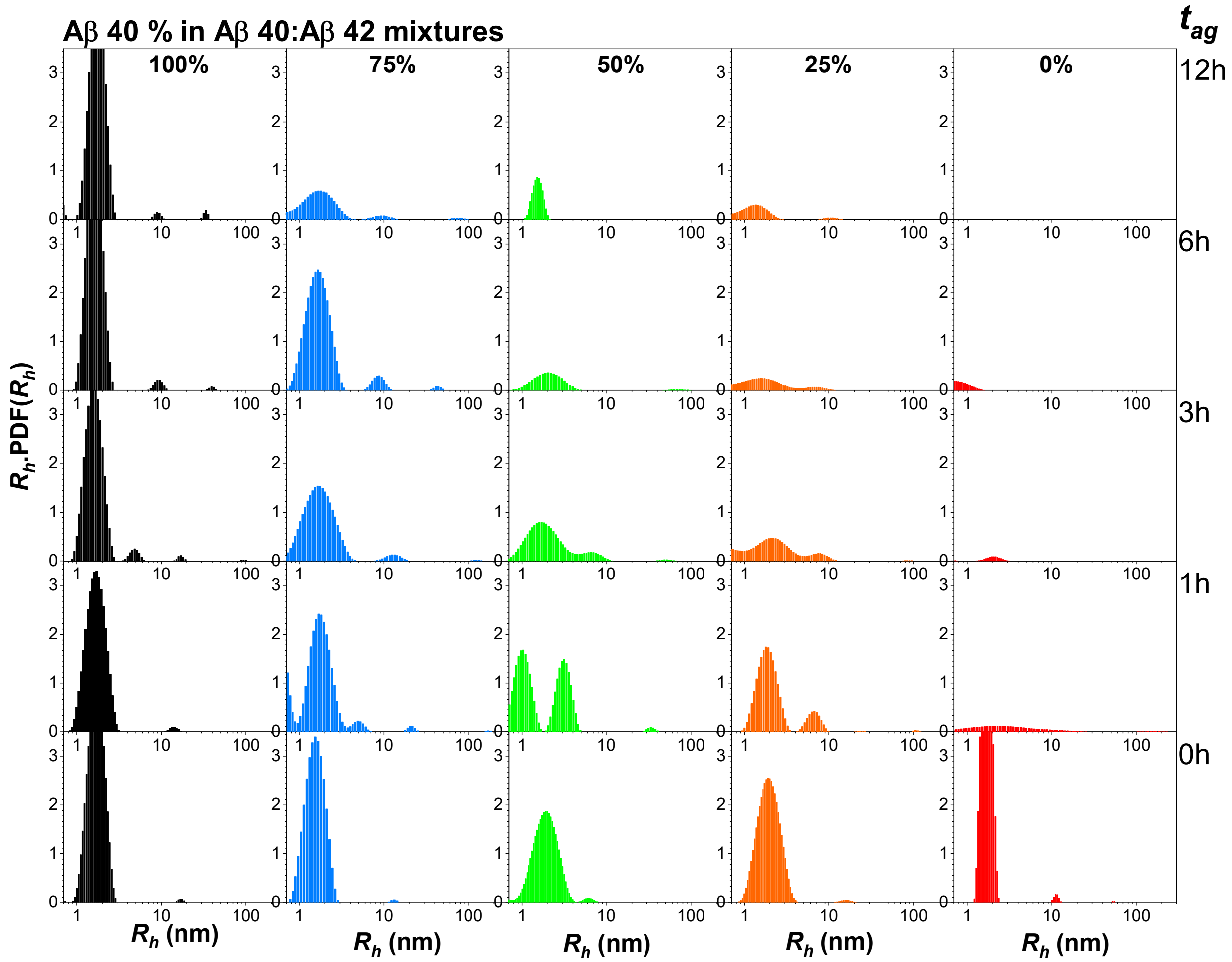

Figure 5. Size distributions of Aβ(1-40):Aβ(1-42) mixtures obtained by CRLI analysis at selected incubation times t_{ag} = 0 to 12 h. Experimental taylorgrams corresponding to these distributions are shown in Figure 1, the experimental conditions are as in Figure 1.

ACKNOWLEDGEMENTS

C.B. acknowledges the funding support from Fonds Wetenschappelijk Onderzoek (grant number G0947.17N) and KU Leuven (grant number C14/18/061). LC thanks the Institut Universitaire de France for support.

AUTHOR CONTRIBUTIONS

Conceptualization – HC and JC designed the experiments. **Investigation** – MD realized the TDA experiments and treated the data. OD realized the AFM experiments. **Methodology** – LC and JC fitted the data with the kinetic equations. **Software** – LC developed the script for the kinetic modelling and the CONTIN TDA data treatment. **Supervision** – JC and HC supervised MD for TDA experiments. JFH supervised MD for peptide synthesis. **Validation** – JC and HC validated and interpreted the TDA results. OD and CB validated and interpreted the AFM results. **Writing – original draft** – JC wrote the first draft and made the figures. OD made figure 3. **Writing – review & editing** – All authors read and edited the manuscript. All authors have given approval to the final version of the manuscript.

Supporting information

Theoretical aspects of TDA, experimental elution profiles, average hydrodynamic radii over the whole aggregation process of each population and for all mixtures; CRLI analysis for all mixtures, and the kinetic fits.

References

1. A. s. Association, *2019 Alzheimer's disease facts and figures*, Report 15525260, 2019.

2. K. Ando, Q. Laborde, A. Lazar, D. Godefroy, I. Youssef, M. Amar, A. Pooler, M.-C. Potier, B. Delatour and C. Duyckaerts, Inside Alzheimer brain with CLARITY: senile plaques, neurofibrillary tangles and axons in 3-D, *Acta Neuropathol.*, 2014, **128**, 457-459. 10.1007/s00401-014-1322-y

3. J. A. Hardy and G. A. Higgins, Alzheimer's disease: the amyloid cascade hypothesis, *Science*, 1992, **256**, 184-185. 10.1126/science.1566067

4. P.-P. Liu, Y. Xie, X.-Y. Meng and J.-S. Kang, History and progress of hypotheses and clinical trials for Alzheimer's disease, *Signal Transduction and Targeted Therapy*, 2019, **4**, 29. 10.1038/s41392-019-0063-8

5. S. V. Salazar and S. M. Strittmatter, Cellular prion protein as a receptor for amyloid-β oligomers in Alzheimer's disease, *Biochem. Biophys. Res. Commun.*, 2017, **483**, 1143-1147. 10.1016/j.bbrc.2016.09.062

6. A. S. König, N. S. Rösener, L. Gremer, M. Tusche, D. Flender, E. Reinartz, W. Hoyer, P. Neudecker, D. Willbold and H. Heise, Structural details of amyloid β oligomers in complex with human prion protein as revealed by solid-state MAS NMR spectroscopy, *J. Biol. Chem.*, 2021, **296**, 100499. https://doi.org/10.1016/j.jbc.2021.100499

7. P. Madhu, D. Das and S. Mukhopadhyay, Conformation-specific perturbation of membrane dynamics by structurally distinct oligomers of Alzheimer's amyloid-β peptide, *PCCP*, 2021, **23**, 9686-9694. 10.1039/D0CP06456D

8. M. J. Guerrero-Muñoz, D. L. Castillo-Carranza, U. Sengupta, M. A. White and R. Kayed, Design of Metastable β-Sheet Oligomers from Natively Unstructured Peptide, *ACS Chem. Neurosci.*, 2013, **4**, 1520-1523. 10.1021/cn4001395

9. P. Arosio, T. P. J. Knowles and S. Linse, On the lag phase in amyloid fibril formation, *PCCP*, 2015, **17**, 7606-7618. 10.1039/c4cp05563b

10. Y.-R. Chen and C. G. Glabe, Distinct Early Folding and Aggregation Properties of Alzheimer Amyloid-β Peptides Aβ40 and Aβ42, *J. Biol. Chem.*, 2006, **281**, 24414-24422. 10.1074/jbc.M602363200

11. M. Novo, S. Freire and W. Al-Soufi, Critical aggregation concentration for the formation of early Amyloid-β (1–42) oligomers, *Sci. Rep.*, 2018, **8**, 1783. 10.1038/s41598-018-19961-3

12. U. Sengupta, A. N. Nilson and R. Kayed, The Role of Amyloid-β; Oligomers in Toxicity, Propagation, and Immunotherapy, *EBioMedicine*, 2016, **6**, 42-49. 10.1016/j.ebiom.2016.03.035

13. J. Wiltfang, H. Esselmann, M. Bibl, M. Hüll, H. Hampel, H. Kessler, L. Frölich, J. Schröder, O. Peters, F. Jessen, C. Luckhaus, R. Perneczky, H. Jahn, M. Fiszer, J. M. Maler, R. Zimmermann, R. Bruckmoser, J. Kornhuber and P. Lewczuk, Amyloid β peptide ratio 42/40 but not Aβ42 correlates with phospho-Tau in patients with low- and high-CSF Aβ40 load, *J. Neurochem.*, 2007, **101**, 1053-1059. https://doi.org/10.1111/j.1471-4159.2006.04404.x

14. J. Hardy, Amyloid, the presenilins and Alzheimer's disease, *Trends Neurosci.*, 1997, **20**, 154-159. 10.1016/S0166-2236(96)01030-2

15. S. W. Snyder, U. S. Ladror, W. S. Wade, G. T. Wang, L. W. Barrett, E. D. Matayoshi, H. J. Huffaker, G. A. Krafft and T. F. Holzman, Amyloid-beta aggregation: selective inhibition of aggregation in mixtures of amyloid with different chain lengths, *Biophys. J.*, 1994, **67**, 1216-1228. https://doi.org/10.1016/S0006-3495(94)80591-0

16. D. Frost, P. M. Gorman, C. M. Yip and A. Chakrabartty, Co-incorporation of Aβ40 and Aβ42 to form mixed pre-fibrillar aggregates, *Eur. J. Biochem.*, 2003, **270**, 654-663. https://doi.org/10.1046/j.1432-1033.2003.03415.x

17. R. Cukalevski, X. Yang, G. Meisl, U. Weininger, K. Bernfur, B. Frohm, T. P. J. Knowles and S. Linse, The Aβ40 and Aβ42 peptides self-assemble into separate homomolecular fibrils in binary mixtures but cross-react during primary nucleation, *Chemical Science*, 2015, **6**, 4215-4233. 10.1039/C4SC02517B

18. L. Gu and Z. Guo, Alzheimer's Aβ42 and Aβ40 form mixed oligomers with direct molecular interactions, *Biochem. Biophys. Res. Commun.*, 2021, **534**, 292-296. https://doi.org/10.1016/j.bbrc.2020.11.092

19. I. Kuperstein, K. Broersen, I. Benilova, J. Rozenski, W. Jonckheere, M. Debulpaep, A. Vandersteen, I. Segers-Nolten, K. Van Der Werf, V. Subramaniam, D. Braeken, G. Callewaert, C. Bartic, R. D'Hooge, I. C. Martins, F. Rousseau, J. Schymkowitz and B. De Strooper, Neurotoxicity of Alzheimer's disease Aβ peptides is induced by small changes in the Aβ42 to Aβ40 ratio, *The EMBO Journal*, 2010, **29**, 3408-3420. https://doi.org/10.1038/emboj.2010.211

20. L. Cerofolini, E. Ravera, S. Bologna, T. Wiglenda, A. Böddrich, B. Purfürst, I. Benilova, M. Korsak, G. Gallo, D. Rizzo, L. Gonnelli, M. Fragai, B. De Strooper, E. E. Wanker and C. Luchinat, Mixing Aβ(1–40) and Aβ(1–42) peptides generates unique amyloid fibrils, *Chem. Commun.*, 2020, **56**, 8830-8833. 10.1039/D0CC02463E

21. K. Hasegawa, I. Yamaguchi, S. Omata, F. Gejyo and H. Naiki, Interaction between Aβ(1−42) and Aβ(1−40) in Alzheimer's β-Amyloid Fibril Formation in Vitro, *Biochemistry*, 1999, **38**, 15514-15521. 10.1021/bi991161m

22. Y. Yan and C. Wang, Aβ40 Protects Non-toxic Aβ42 Monomer from Aggregation, *J. Mol. Biol.*, 2007, **369**, 909-916. https://doi.org/10.1016/j.jmb.2007.04.014

23. K. Pauwels, T. L. Williams, K. L. Morris, W. Jonckheere, A. Vandersteen, G. Kelly, J. Schymkowitz, F. Rousseau, A. Pastore, L. C. Serpell and K. Broersen, Structural Basis for Increased Toxicity of Pathological Aβ42:Aβ40 Ratios in Alzheimer Disease*, *J. Biol. Chem.*, 2012, **287**, 5650-5660. https://doi.org/10.1074/jbc.M111.264473

24. J. Chamieh and H. Cottet, in *Colloid and Interface Science in Pharmaceutical Research and Development*, eds. H. Ohshima and K. Makino, Elsevier, Amsterdam, 2014, DOI: 10.1016/B978-0-444-62614-1.00009-0, pp. 173-192.

25. G. Taylor, The Dispersion of Matter in Turbulent Flow through a Pipe, *Proc R Soc Lon Ser-A*, 1954, **223**, 446-468. https://doi.org/10.1098/rspa.1954.0130

26. G. Taylor, Dispersion of Soluble Matter in Solvent Flowing Slowly through a Tube, *Proc R Soc Lon Ser-A*, 1953, **219**, 186-203. https://doi.org/10.1098/rspa.1953.0139

27. M. Deleanu, J. F. Hernandez, L. Cipelletti, J. P. Biron, E. Rossi, M. Taverna, H. Cottet and J. Chamieh, Unraveling the Speciation of beta-Amyloid Peptides during the Aggregation Process by Taylor Dispersion Analysis, *Anal. Chem.*, 2021, **93**, 6523-6533. 10.1021/acs.analchem.1c00527

28. A. Hawe, W. Hulse, W. Jiskoot and R. Forbes, Taylor Dispersion Analysis Compared to Dynamic Light Scattering for the Size Analysis of Therapeutic Peptides and Proteins and Their Aggregates, *Pharm. Res.*, 2011, **28**, 2302-2310. https://doi.org/10.1007/s11095-011-0460-3

29. H. Cottet, J. P. Biron and M. Martin, Taylor Dispersion Analysis of Mixtures, *Anal. Chem.*, 2007, **79**, 9066-9073. 10.1021/ac071018w

30. M. S. Bello, R. Rezzonico and P. G. Righetti, Use of Taylor-Aris Dispersion for Measurement of a Solute Diffusion Coefficient in Thin Capillaries, *Science*, 1994, **266**, 773-776. https://doi.org/10.1126/science.266.5186.773

31. U. Sharma, N. J. Gleason and J. D. Carbeck, Diffusivity of Solutes Measured in Glass Capillaries Using Taylor's Analysis of Dispersion and a Commercial CE Instrument, *Anal. Chem.*, 2005, **77**, 806-813. 10.1021/ac048846z

32. H. Cottet, M. Martin, A. Papillaud, E. Souaïd, H. Collet and A. Commeyras, Determination of Dendrigraft Poly-l-Lysine Diffusion Coefficients by Taylor Dispersion Analysis, *Biomacromolecules*, 2007, **8**, 3235-3243. https://doi.org/10.1021/bm070268j

33. F. d'Orlyé, A. Varenne and P. Gareil, Determination of nanoparticle diffusion coefficients by Taylor dispersion analysis using a capillary electrophoresis instrument, *J. Chromatogr. A*, 2008, **1204**, 226-232. 10.1016/j.chroma.2008.08.008

34. J. Chamieh, H. Merdassi, J.-C. Rossi, V. Jannin, F. Demarne and H. Cottet, Size characterization of lipid-based self-emulsifying pharmaceutical excipients during lipolysis using Taylor dispersion analysis with fluorescence detection, *Int. J. Pharm.*, 2018, **537**, 94-101. https://doi.org/10.1016/j.ijpharm.2017.12.032

35. D. A. Urban, A. M. Milosevic, D. Bossert, F. Crippa, T. L. Moore, C. Geers, S. Balog, B. Rothen-Rutishauser and A. Petri-Fink, Taylor Dispersion of Inorganic Nanoparticles and Comparison to Dynamic Light Scattering and Transmission Electron Microscopy, *Colloid and Interface Science Communications*, 2018, **22**, 29-33. https://doi.org/10.1016/j.colcom.2017.12.001

36. M. E. Pedersen, J. Østergaard and H. Jensen, Flow-Induced Dispersion Analysis (FIDA) for Protein Quantification and Characterization, *Methods Mol. Biol.*, 2019, **1972**, 109-123. 10.1007/978-1-4939-9213-3_8

37. R. Verpillot, M. Otto, H. Klafki and M. Taverna, Simultaneous analysis by capillary electrophoresis of five amyloid peptides as potential biomarkers of Alzheimer's disease, *J. Chromatogr. A*, 2008, **1214**, 157-164. https://doi.org/10.1016/j.chroma.2008.10.051

38. D. Brinet, J. Kaffy, F. Oukacine, S. Glumm, S. Ongeri and M. Taverna, An improved capillary electrophoresis method for in vitro monitoring of the challenging early steps of Aβ(1-42) peptide oligomerization: Application to anti-Alzheimer's drug discovery, *Electrophoresis*, 2014, **35**, 3302-3309. 10.1002/elps.201400271

39. J. Chamieh and H. Cottet, in *Colloid and Interface Science in Pharmaceutical Research and Development*, eds. H. Ohshima and K. Makino, Elsevier, Amsterdam, 2014, DOI: https://doi.org/10.1016/B978-0-444-62614-1.00009-0, pp. 173-192.

40. L. Cipelletti, J.-P. Biron, M. Martin and H. Cottet, Measuring Arbitrary Diffusion Coefficient Distributions of Nano-Objects by Taylor Dispersion Analysis, *Anal. Chem.*, 2015, **87**, 8489-8496. 10.1021/acs.analchem.5b02053

41. D. Nečas and P. Klapetek, Gwyddion: an open-source software for SPM data analysis, *Open Physics*, 2012, **10**, 181-188. 10.2478/s11534-011-0096-2

42. C. A. Schneider, W. S. Rasband and K. W. Eliceiri, NIH Image to ImageJ: 25 years of image analysis, *Nature Methods*, 2012, **9**, 671-675. 10.1038/nmeth.2089

43. J. Chamieh, L. Leclercq, M. Martin, S. Slaoui, H. Jensen, J. Østergaard and H. Cottet, Limits in Size of Taylor Dispersion Analysis: Representation of the Different Hydrodynamic Regimes and Application to the Size-Characterization of Cubosomes, *Anal. Chem.*, 2017, **89**, 13487-13493. https://doi.org/10.1021/acs.analchem.7b03806

44. H. Cottet, J. P. Biron and M. Martin, On the optimization of operating conditions for Taylor dispersion analysis of mixtures, *Analyst*, 2014, **139**, 3552-3562. https://doi.org/10.1039/C4AN00192C

45. P. Vedula and P. K. Yeung, Similarity scaling of acceleration and pressure statistics in numerical simulations of isotropic turbulence, *Physics of Fluids*, 1999, **11**, 1208-1220. 10.1063/1.869893

46. G. Meisl, X. Yang, E. Hellstrand, B. Frohm, J. B. Kirkegaard, S. I. A. Cohen, C. M. Dobson, S. Linse and T. P. J. Knowles, Differences in nucleation behavior underlie the contrasting aggregation kinetics of the Aβ40 and Aβ42 peptides, *Proc. Natl. Acad. Sci. U. S. A.*, 2014, **111**, 9384. 10.1073/pnas.1401564111

47. O. Deschaume, B. De Roo, M. J. Van Bael, J.-P. Locquet, C. Van Haesendonck and C. Bartic, Synthesis and Properties of Gold Nanoparticle Arrays Self-Organized on Surface-Deposited Lysozyme Amyloid Scaffolds, *Chem. Mater.*, 2014, **26**, 5383-5393. 10.1021/cm502652t

48. A. T. Winzer, C. Kraft, S. Bhushan, V. Stepanenko and I. Tessmer, Correcting for AFM tip induced topography convolutions in protein–DNA samples, *Ultramicroscopy*, 2012, **121**, 8-15. https://doi.org/10.1016/j.ultramic.2012.07.002

49. C. Godon, J.-M. Teulon, M. Odorico, C. Basset, M. Meillan, L. Vellutini, S.-w. W. Chen and J.-L. Pellequer, Conditions to minimize soft single biomolecule deformation when imaging with atomic force microscopy, *J. Struct. Biol.*, 2017, **197**, 322-329. https://doi.org/10.1016/j.jsb.2016.12.011

50. Y. Xing, A. Nandakumar, A. Kakinen, Y. Sun, T. P. Davis, P. C. Ke and F. Ding, Amyloid Aggregation under the Lens of Liquid–Liquid Phase Separation, *The Journal of Physical Chemistry Letters*, 2021, **12**, 368-378. 10.1021/acs.jpclett.0c02567

51. Y. Nakasone and M. Terazima, A Time-Resolved Diffusion Technique for Detection of the Conformational Changes and Molecular Assembly/Disassembly Processes of Biomolecules, *Frontiers in Genetics*, 2021, **12**. 10.3389/fgene.2021.691010

52. S. Brocca, R. Grandori, S. Longhi and V. Uversky, Liquid–Liquid Phase Separation by Intrinsically Disordered Protein Regions of Viruses: Roles in Viral Life Cycle and Control of Virus–Host Interactions, *Int. J. Mol. Sci.*, 2020, **21**, 9045. 10.3390/ijms21239045

53. S. S. Kwak, K. J. Washicosky, E. Brand, D. von Maydell, J. Aronson, S. Kim, D. E. Capen, M. Cetinbas, R. Sadreyev, S. Ning, E. Bylykbashi, W. Xia, S. L. Wagner, S. H. Choi, R. E. Tanzi and D. Y. Kim, Amyloid-β42/40 ratio drives tau pathology in 3D human neural cell culture models of Alzheimer's disease, *Nature Communications*, 2020, **11**, 1377. 10.1038/s41467-020-15120-3

54. A. J. Dear, T. C. T. Michaels, G. Meisl, D. Klenerman, S. Wu, S. Perrett, S. Linse, C. M. Dobson and T. P. J. Knowles, Kinetic diversity of amyloid oligomers, *Proc. Natl. Acad. Sci. U. S. A.*, 2020, **117**, 12087-12094. 10.1073/pnas.1922267117

55. P. Virtanen, R. Gommers, T. E. Oliphant, M. Haberland, T. Reddy, D. Cournapeau, E. Burovski, P. Peterson, W. Weckesser, J. Bright, S. J. van der Walt, M. Brett, J. Wilson, K. J. Millman, N. Mayorov, A. R. J. Nelson, E. Jones, R. Kern, E. Larson, C. J. Carey, İ. Polat, Y. Feng, E. W. Moore, J. VanderPlas, D. Laxalde, J. Perktold, R. Cimrman, I. Henriksen, E. A. Quintero, C. R. Harris, A. M. Archibald, A. H. Ribeiro, F. Pedregosa, P. van Mulbregt, A. Vijaykumar, A. P. Bardelli, A. Rothberg, A. Hilboll, A. Kloeckner, A. Scopatz, A. Lee, A. Rokem, C. N. Woods, C. Fulton, C. Masson, C. Häggström, C. Fitzgerald, D. A. Nicholson, D. R. Hagen, D. V. Pasechnik, E. Olivetti, E. Martin, E. Wieser, F. Silva, F. Lenders, F. Wilhelm, G. Young, G. A. Price, G.-L. Ingold, G. E. Allen, G. R. Lee, H. Audren, I. Probst, J. P. Dietrich, J. Silterra, J. T. Webber, J. Slavič, J. Nothman, J. Buchner, J. Kulick, J. L. Schönberger, J. V. de Miranda Cardoso, J. Reimer, J. Harrington, J. L. C. Rodríguez, J. Nunez-Iglesias, J. Kuczynski,

K. Tritz, M. Thoma, M. Newville, M. Kümmerer, M. Bolingbroke, M. Tartre, M. Pak, N. J. Smith, N. Nowaczyk, N. Shebanov, O. Pavlyk, P. A. Brodtkorb, P. Lee, R. T. McGibbon, R. Feldbauer, S. Lewis, S. Tygier, S. Sievert, S. Vigna, S. Peterson, S. More, T. Pudlik, T. Oshima, T. J. Pingel, T. P. Robitaille, T. Spura, T. R. Jones, T. Cera, T. Leslie, T. Zito, T. Krauss, U. Upadhyay, Y. O. Halchenko, Y. Vázquez-Baeza and C. SciPy, SciPy 1.0: fundamental algorithms for scientific computing in Python, *Nature Methods*, 2020, **17**, 261-272. 10.1038/s41592-019-0686-2

56. G. Meisl, J. B. Kirkegaard, P. Arosio, T. C. T. Michaels, M. Vendruscolo, C. M. Dobson, S. Linse and T. P. J. Knowles, Molecular mechanisms of protein aggregation from global fitting of kinetic models, *Nat. Protoc.*, 2016, **11**, 252-272. 10.1038/nprot.2016.010

57. S. I. A. Cohen, S. Linse, L. M. Luheshi, E. Hellstrand, D. A. White, L. Rajah, D. E. Otzen, M. Vendruscolo, C. M. Dobson and T. P. J. Knowles, Proliferation of amyloid-β42 aggregates occurs through a secondary nucleation mechanism, *Proc. Natl. Acad. Sci. U. S. A.*, 2013, **110**, 9758-9763. 10.1073/pnas.1218402110

58. A. J. Dear, G. Meisl, A. Šarić, T. C. T. Michaels, M. Kjaergaard, S. Linse and T. P. J. Knowles, Identification of on- and off-pathway oligomers in amyloid fibril formation, *Chemical Science*, 2020, **11**, 6236-6247. 10.1039/C9SC06501F

59. G. Bitan, M. D. Kirkitadze, A. Lomakin, S. S. Vollers, G. B. Benedek and D. B. Teplow, Amyloid β-protein (Aβ) assembly: Aβ40 and Aβ42 oligomerize through distinct pathways, *Proc. Natl. Acad. Sci. U. S. A.*, 2003, **100**, 330-335. 10.1073/pnas.222681699

For TOC Only:

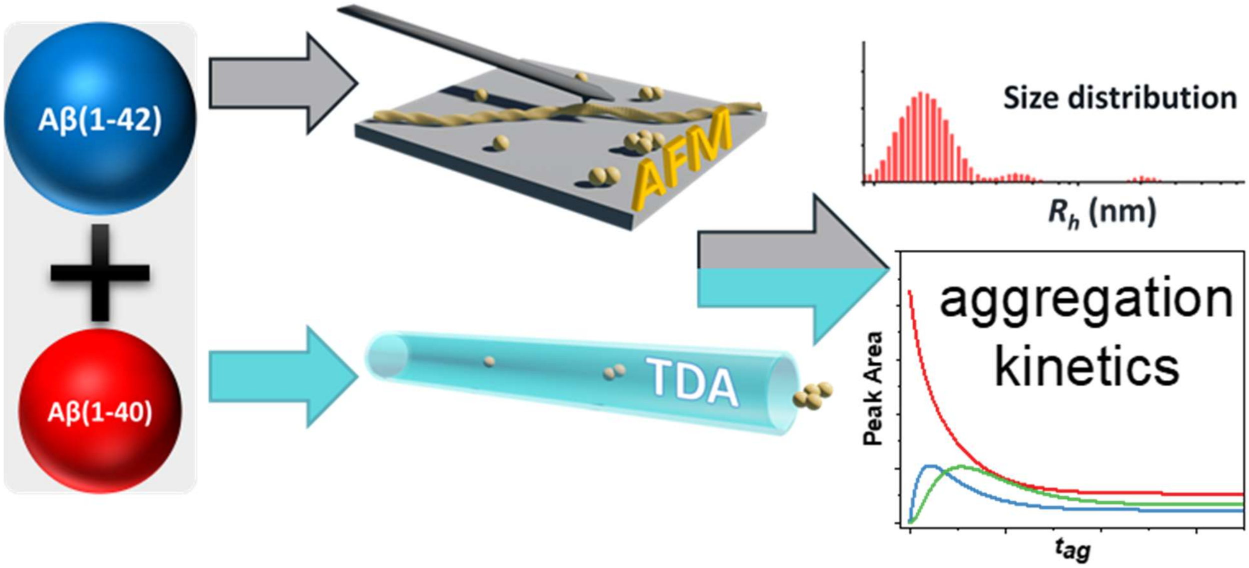
Aβ(1-42)
Aβ(1-40)
AFM
TDA
Size distribution
R_h (nm)
aggregation kinetics
Peak Area
t_{ag}